Effect of Unsteady Separation on an Automotive Bluff-Body In Cross-Wind

M. Gohlke[1,2], J.F. Beaudoin[1], M. Amielh[2] and F. Anselmet[2]

[1] *PSA Peugeot-Citroën, Department of Research and Innovation, Vélizy-Villacoublay, France*
[2] *IRPHE, UMR CNRS 6594, Technopôle de Château-Gombert, Marseille, France*
marc.gohlke@mpsa.com

Abstract. This paper is treating the dynamic effects of cross-wind on a 3D bluff-body. It is shown that contrary to the mean flow, it is not the upper vortex that predominates the forces, but the flow generated and piloted by the front lee-strut wake. It is made responsible for the appearance of a frequency peak in the bluff-body force spectra. Furthermore it is shown that the intensity as well as the frequency of this peak depend on the yawing angle. Experimental and numerical results are used to analyse the flow dynamics.

Key words: cross-wind, aerodynamics, bluff-body, vortices, wake.

1. Introduction

During many years automobile aerodynamic research was concentrated on drag-reduction and some major advances have been achieved. However, a new topic has emerged recently. As consumers demand bigger interior, cars become higher and larger. This leads to more side wind sensibility. Hence, it is necessary to understand the link between side-force, yawing-moment and rolling-moment, so that the driving-stability and -comfort can be enhanced.

Howell (1993) and Gillhaus & Hoffmann (1998) have shown that in automobile applications it is essentially the side force and its repartition, causing the yawing moment, that are responsible for driving stability.

The aim of the present study is to get some insight into the flow-structures that have an influence on these forces, which is a fundamental question that concerns many fields beyond the automotive aerodynamics community. To reduce the complexity of the flow around a vehicle in cross-wind a simplified bluff-body in ground-proximity, introduced by Chometon et al. (2004), has been chosen for a more generic analysis. Figure 1 shows the model, "Willy", used for the present study, with the forces and moments in their reference system.

In a cross wind situation the flow around this bluff body is basically characterised by its asymmetry, which is at the origin of additional forces and moments, namely side force and yawing moment.

This paper mainly aims at giving some insight to the dynamics of the forces and their link to the flow structures. First of all a summary of the principal results, obtained from the steady flow analysis, are presented. In the main part, devoted to the unsteady character of the flow, first a brief description of the numerical simulation and the experimental setup is given. Some results obtained from these investigations are then analysed and finally the influence of the flow structures is discussed.

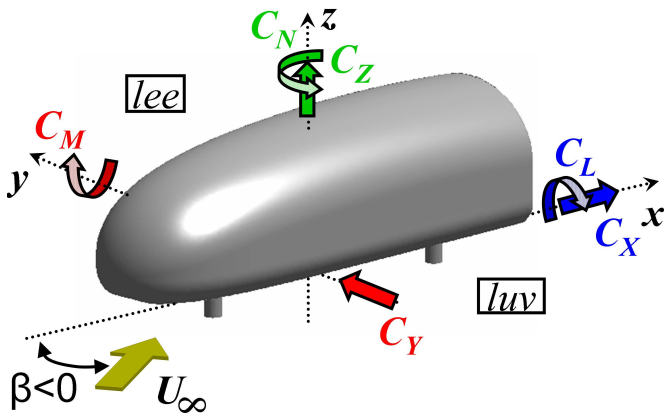

Figure 1. Coordinate system and forces as applied to the bluff-body used for investigation, over all length used as reference length: L_{ref}

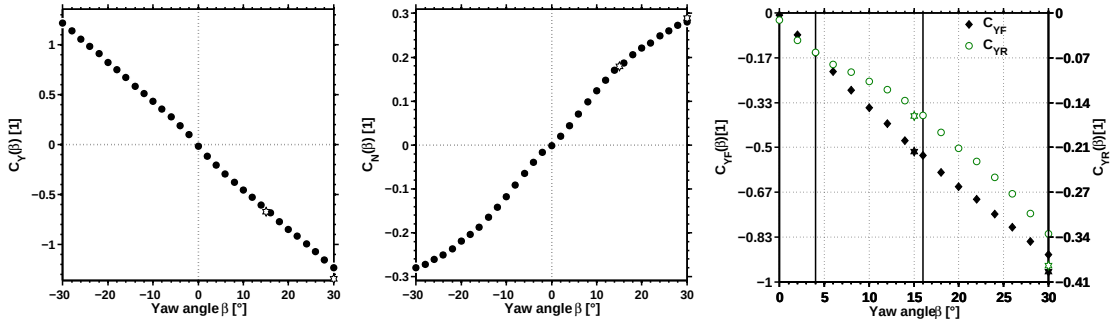

(a) global side force C_Y (b) Yawing moment C_N (c) Front and rear side-force C_{YF},C_{YR}

Figure 2. Steady force coeffi cient as a function of yaw angle β (*stars* : numerical simulation)

2. Recapitulation of mean flow features

In this section the main features of the steady fbw field are presented. A more exhaustive overview of these results can be found in Gohlke et al. (2007). As mentioned in the introduction, the main interest is turned toward the side force distribution and the resulting yawing moment. To simulate cross wind, a simple but often applied method is used. The wind tunnel model is therefore turned in respect to the free stream by an angle β, called the yaw angle. As this angle rises, the component of the oncoming fbw becomes more important, simulating a stronger cross wind. In this study, the maximum yaw angle is 30° and the upstream velocity is 40m/s.

Figure 2 shows the strong dependency of forces and moments on the yawing angle. While the global side force (Figure 2(a)) has a rather linear rise, the slope of the yawing moment C_N (Figure 2(b)) shows an inclination at around 16°, which, as discussed in the introduction, is favourable for cross-wind stability. To clarify the origin of this decrease, the lateral force is divided into front and rear side forces (Figure 2(c)), which leads to the following two observations. The front contribution C_{YF} is three times higher but it is the rear side force C_{YR} that shows two slope changes, at 4° and 16°. The second one, occurring at yaw angles above 16°, leads to a steeper slope which is thought to partially explain the decrease in yawing moment. In Gohlke et al. (2007) these two slope changes

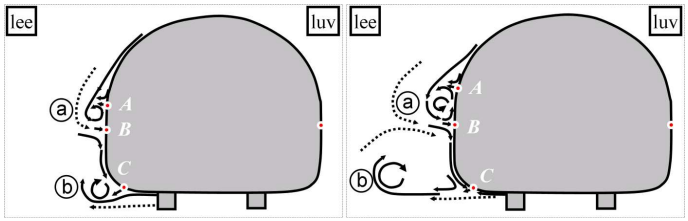

Figure 3. Lee side flow for $\beta < 20\,^{\circ}$(left) and $\beta > 20^{\circ}$ (right)

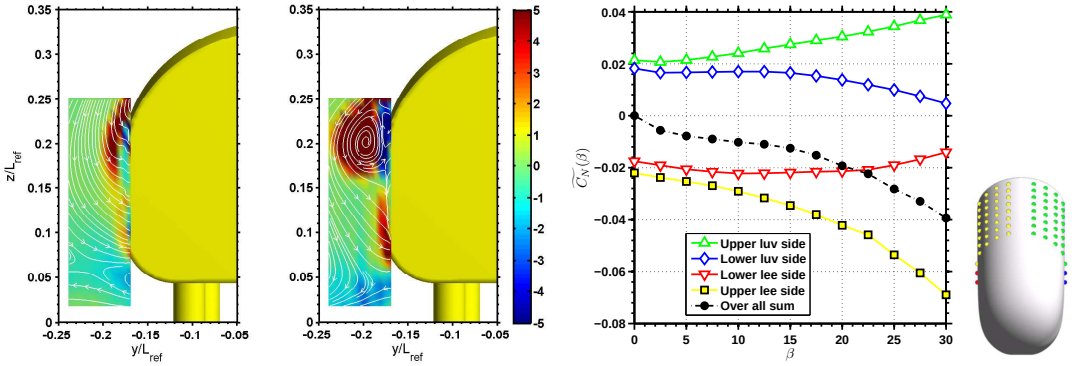

(a) $\beta = 15^{\circ}$ (b) $\beta = 30^{\circ}$ (c) $\widetilde{C_N}$ pseudo-yawing moment on the rear part of the model

Figure 4. LDV measurements and local yawing moment contributions on the rear half of the model

are linked to the presence of two vortices (a) and (b) as shown by the sketch in Figure 3.

The vortex (b) is close to the body at small yaw angles and induces low pressure at the rear end of the model. As β grows, this flow structure gains in size but is also orientated away from the body, hence it has less influence on the rear side force. The front strut wake plays herein an important role by imposing a direction to this vortex. At yaw angles around 15° a second vortex (a) is created, due to detachment of the flow over the top. This vortex grows in size, as visible on the LDV-measurements shown in Figures 4(a) and 4(b), and induces a low pressure zone on the rear lee side, giving rise in C_{YR}, and finally leading to a counter-rotating rear yawing moment. This local effect is shown in Figure 4(c), which is obtained from local static pressure measurements and has permitted the calculation of force contributions per region. It can be observed that the strongest gain in local yawing moment $\widetilde{C_N}$ is measured on the rear upper leeward side (□).

Figures 5(a) and 5(b) give an overview of the mean flow field of the lee side at $15\,^{\circ}$ and 30° as obtained from numerical simulations. They illustrate the presence of the longitudinal vortices and their location in respect to the model.

3. Unsteady flow analysis

3.1. Setup

In this section the setup used to analyse the unsteady character of the flow is presented. First the numerical method employed and its setup is discussed and then the experimental method is outlined. The upstream flow velocity in both cases is 40m/s. To simulate a cross flow, the model is turned around its z-axis at the strut centre in respect to the oncoming

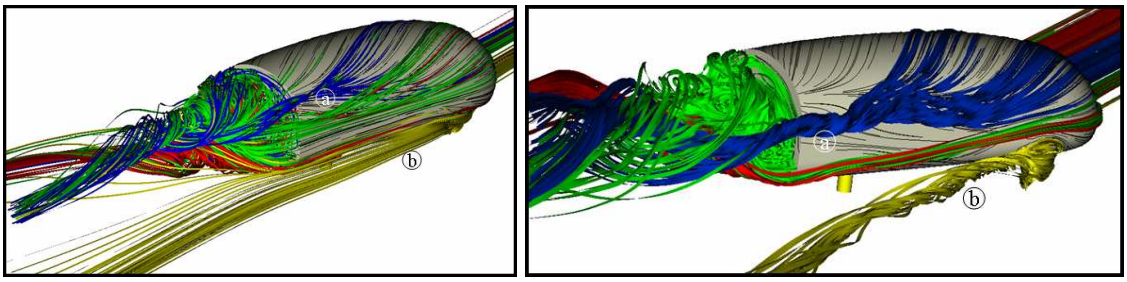

(a) Bluff-body flow at $\beta = 15\,^{\circ}$ (b) Bluff-body flow at $\beta = 30\,^{\circ}$

Figure 5. Lee-ward side view of the mean flow field for 15° and 30° yaw, obtained from numerical simulation

flow up to a yaw angle of $\pm 30\,^{\circ}$.

Numerical investigation The numerical code used in this investigation is based on a lattice Boltzmann method. Two yaw angles have been studied, one at $15°$ and one at $30°$. Different zones of spatial resolution are used, the finest grid being close to the model and around the cylindrical struts of the order of magnitude of $0.875 \times 10^{-6} L_{ref}$. In the $30°$ case a special refinement of $1.75 \times 10^{-6} L_{ref}$ is done in the zone of the lateral vortices on the lee side. This zone is defined by the iso-surface of the vorticity norm, obtained from an earlier coarser numerical investigation. The total number of voxels used to define the flow field is of the order of $10^{\,7}$.

1.4×10^5 timesteps are simulated for both yaw angles, which correspond to a physical time of 0.56s. To find a converged behaviour drag-, side-force- and lift coefficients are monitored and it is found that 2×10^4 timesteps are necessary to consider the simulation as converged. This leaves 0.48s of physical time for dynamic flow analysis. The turbulence level and the boundary layer are adapted to fit the conditions in the wind tunnel experiments.

The numerical simulation is confronted with experimental results and globally show a satisfactory correspondence. Exemplarily some of these confrontations are given here. The force measurements in Figure 2 show that the steady forces are well reproduced (the numerical results are displayed by the stars). At the high yaw angle, the side force is slightly over estimated by the simulation with a difference of $\Delta C_Y = 8.8\%$, but the front/rear distribution is well respected, which is confirmed by a good C_N estimation differing by $\Delta C_N = 1.4\%$. A further confirmation of good coherence comes from the LDV measurements in a plane close to the blunt end. The vorticity level as well as the roll-up of the streamlines is quite similar for the $30°$ case, shown in Figures 6(a) and 6(b).

It is therefore stated, that the numerical simulation gives accurate results and can be amended with the experimental investigation, which is completer in angular resolution.

Experimental investigation One half of the hollow experimental model is equipped with 249 pressure holes with a diameter of 0.8mm. They can be equipped with microphones to analyse local pressure fluctuation. The microphones are fixed on the inside of the model with the help of tight joints, that are glued to the shell.

The measuring equipment used is capable to analyse 60 microphones at a time. Three different setups are hence used: one covering the upper part, one covering the lower part

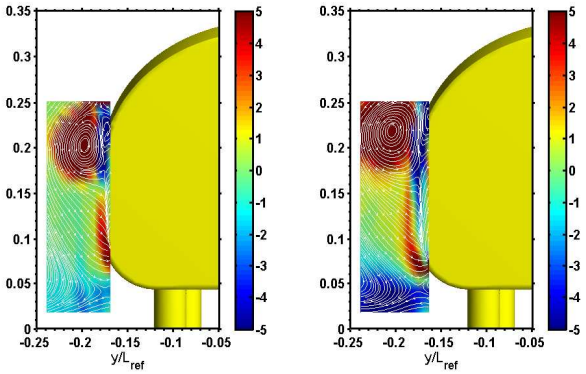

(a) LDV measurements 30° (b) Numerical simulation 30°

Figure 6. Vorticity in a plane obtained from LDV measurements and from numerical simulation at 30° yaw

and a combination of both of them (see Figure 7). This investigation has been under-

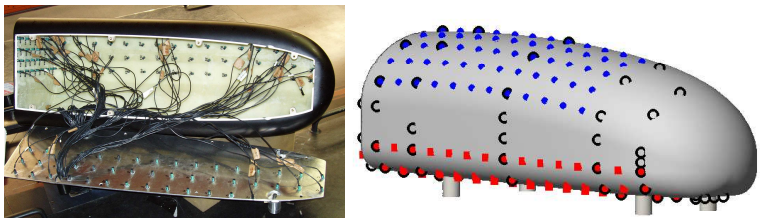

(a) Wind tunnel model equipped with pressure transducers (b) Three different measurement series : •, ■ and ○

Figure 7. Model equipped with pressure transducers and their position during the different setups

taken for a yaw angle range between -30° and $+30^\circ$ with a step of 5° at a measurement frequency of 8kHz.

3.2. RESULTS & DISCUSSION

It has been shown that the steady flow is mainly characterised by two longitudinal vortices on the lee side of the model and that they play an important role in the local side force and local yawing moment distributions (see Section 2.). In this section, further results are presented, that aim at understanding the dynamics of the side force C_Y and the yawing moment C_N. These results are based on two different approaches, on the one hand, a numerical simulation gives access to the unsteady forces and a very good spatial resolution. But, on the other hand, good yaw angle resolution can only be achieved with an experimental approach, where pressure fluctuations are measured on the model surface. These two setups are described in Section 3.1.

Numerical investigation To analyse the dynamics of the forces, numerical simulations were undertaken for two different yaw angles, 15° and 30°. As shown in section 3.1. the comparison between the wind tunnel measurements and the numerical simulation is satisfactory. It can be seen that the steady forces and moments of the numerical simulation correspond fairly well. This is demonstrated by the stars in the forces versus yaw angle

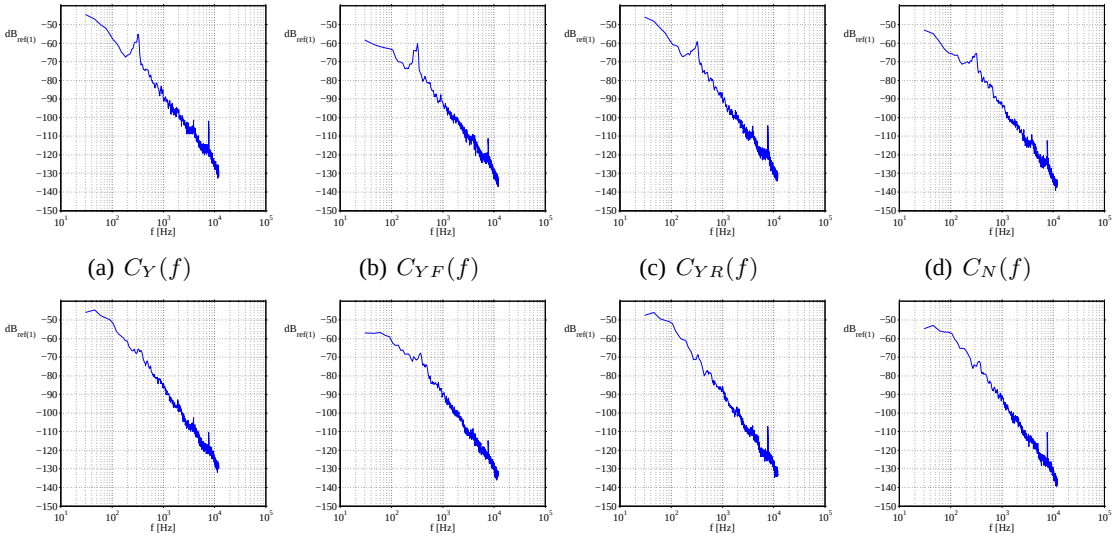

(a) $C_Y(f)$ (b) $C_{YF}(f)$ (c) $C_{YR}(f)$ (d) $C_N(f)$

(e) $C_Y(f)$ (f) $C_{YF}(f)$ (g) $C_{YR}(f)$ (h) $C_N(f)$

Figure 8. Force spectra for $15°$ (a-d) and $30°$ case (e-h)

graphs in Figure 2. On the bases of this good correlation between the numerical simulation and the wind tunnel measurements for the steady flow, it is assumed that the unsteady analysis using the numerical data will also produce reliable results.

Force autospectra obtained from the numerical simulation of the $15°$ case and $30°$ case, as shown in Figure 8 for the side force and the yawing moment, display overall simplicity. A first observation is the resemblance of these spectra between the two yaw angles. The spectra globally have the same energy level. At high frequencies they follow a power law, typical for generic turbulent flows, but the slope value of -4, could not be explained so far. Furthermore, all spectra display a frequency peak emergence, which is easiest to distinguish for the small yaw angle. These peaks have an amplitude that is about 10dB higher for the $15°$ case than for the $30°$ case. Furthermore, these frequencies vary with yaw, most visible on the front side force, where $f_{15°}^{C_{YF}}$ =317Hz and $f_{30°}^{C_{YF}}$ =363Hz.

To analyse the origin of this coherent part of the spectra, indications can be obtained from local force analysis undertaken on the cylindrical struts. They are shown in Figure 9. Again, at high frequencies, the spectra show a decrease following a power law. Generally, peaks with identical frequencies, as observed for the whole body, emerge clearly at both yaw angles. The amplitude of the frequency peak is higher and the peaks are slimmer for the $15°$ case.

The global and the front side force again show a variation of the frequency which depends on the yaw angle: $f_{15°}$ =317Hz and $f_{30°}$ =363Hz. Only the frequency on the rear struts is independent of the yaw angle change: $f_{15°} = f_{30°}$ =317Hz.

Due to the fact that there is a strong coherent phenomenon in the spectra, with the same frequency as observed on the body force spectra, it is believed that the struts are at the origin of these frequencies. This can be explained by vortices shed in their wake, similar to the ”von Karman vortex street”. This shedding is thought to induce its proper frequency on the body, by an alternation of local low and high pressure zones close to the body surface.

The spectrum of C_{YF} is presented in Figure 9(d), it has been obtained only from the force on the body (without the contribution from the struts). Again the frequency peak

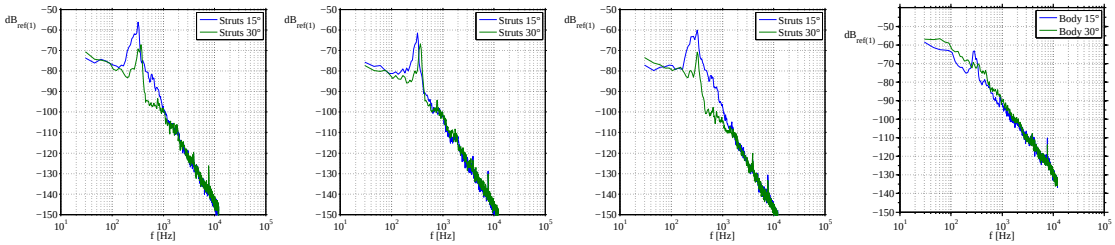

(a) $C_Y(f)$ on struts (b) $C_{YF}(f)$ on struts (c) $C_{YR}(f)$ on struts (d) $C_{YF}(f)$ on body

Figure 9. Force spectra of the cylindrical struts and of the body for $15°$ and $30°$ case

can be observed, which underlines the influence of the strut wake on the body forces.

A first attempt is to verify whether the order of magnitude corresponds to the vortex shedding frequency of a cylinder. This is done by a simple comparison through the Strouhal number. The corresponding shedding frequency is calculated with the dimensions of the cylindrical struts and a Strouhal number of $St = 0.21$ (for a $Re = U_\infty D/\nu = 10^3\, to\, 3\times10^6$). The local Reynolds number being $Re(U_\infty, d) = 8.2\times10^4$ this corresponds to $f = 274.5$Hz. A detailed look at the oncoming flow velocity is shown in Figure 10. It can be seen that the flow velocity upstream of the lee strut is at first slowed down, due to a blockage effect of the model, before it is strongly accelerated due to the curvature on the model nose, generating a convergent effect. So the velocity to be taken into account to estimate the vortex shedding frequency is about 10m/s higher than the actual free stream velocity, so that the obtained frequency is about 343Hz, corresponding to the $30°$ yaw angle. This is to be compared with $f_{30°}^{C_{YF}} = 363$Hz and shows a good agreement.

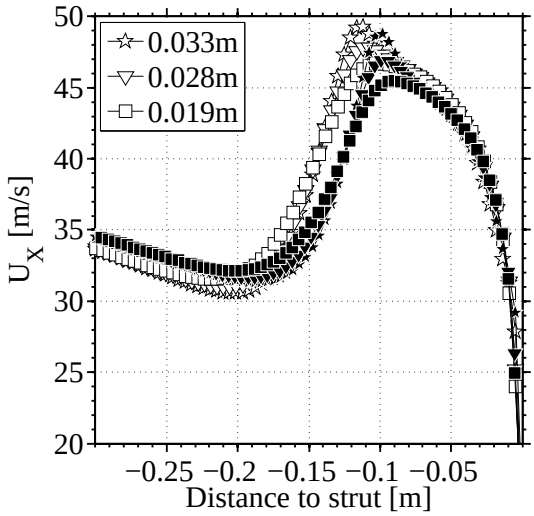

Figure 10. Oncoming flow U_X at different heights z for $15°$ (filled) and $30°$ (empty) - ground clearance g=0.037m

This comforts the idea that the vortex shedding from the leeward strut is responsible for the peaks found on the force spectra. Figure 10 also shows that the oncoming flow velocity changes with the yaw angle, leading to a change in the shedding frequency. The authors believe that this explains in part the variation of the frequency of the coherent phenomena observed in the spectra; but other factors such as the model geometry behind

the strut might favour an acceleration of the strut wake, which then also influences the resulting frequency.

Experimental investigation The numerical investigation suggests that there is a yaw angle dependency of the coherent part of force spectra, showing frequency changes and amplitude variations. With the help of surface pressure measurements, as described in Section 3.1., an analysis can be undertaken over the whole yaw angle range from -30° to +30°, with a step of 5°.

The spectral analysis of the results from these local pressure measurements is shown in Figure 11. Exemplarily, four different transducers 30, 31, 32 and 37 are analysed for the yaw angles between $0°$ to $30°$ (lee side).

First of all, it has to be pointed out that these transducers are not only sensitive to turbulent fluctuations, but also to acoustic noise. The wind tunnel, being equipped with four turbines downstream of the model, generates a noise with a frequency of 86Hz for a wind velocity of 40m/s. Black lines in the illustrated graphs indicate this frequency and its harmonics, so that they can be clearly distinguished. It can be stated that their amplitude stays below 100dB. Flow analysis will nevertheless be restricted to frequencies that do not correspond to these acoustic frequencies. A further observation on these measurements is a broad band bump in the spectra at frequencies around 2kHz. This is explained by the way the transducers are installed and corresponds to resonance frequencies of the cavity between the outer shell of the model and the transducer. This frequency can vary slightly with the location and the fixation of the transducer.

Figure 11(a-c) reproduces the results from three different pressure transducer at different heights on the lee ward side, No 30 being the lowest, placed on the horizontal underbody, as indicated in Figure 12(a).

This transducer No. 30 shows a yaw angle independent energy level. The further the transducer is located upward the lateral side of the model, the more this level depends on the yaw angle. Figure 11(b) shows a dependency up to a yaw angle of $10°$, beyond the energy levels remain constant. A strong dependency of this level on the yaw angle is demonstrated by transducer No. 32. It can also be pointed out that at 30° yaw the global energy level is the same for all the positions. This means that the lateral side is more and more subject to the flow fluctuation and the lateral turbulence level rises constantly with the yaw angle, as a large lateral wake is building up. Furthermore, these spectra show a slope at high frequency of -7/3, this spectral decrease has often been observed on pressure measurements in homogeneous and isotropic turbulence.

Most of the spectra show clear peaks at frequencies between 270Hz and 300Hz with an amplitude mostly above 100dB. Although this is not exactly the same value as observed in the numerical simulation, these frequencies are rather close. As already observed on the force spectra, the amplitudes and the corresponding frequencies, obtained from the pressure transducers, vary with the yaw angle. Figures 12(b) and 12(c) show this behaviour exemplarily for the transducers No. 31 and 37, the later one being just behind the front lee side strut (see Figure 12(a)) and therefore measuring in its wake.

It can be observed that at low β the frequency and the amplitude rise with the yaw angle. The amplitude reaches its maximum for $10°$ to $15°$, where the frequency attains a value of around 290Hz. While the amplitude decreases with a further rise in yaw angle, the frequency seems established around 295Hz.

In addition to this, there is a further frequency bump arising around a frequency of

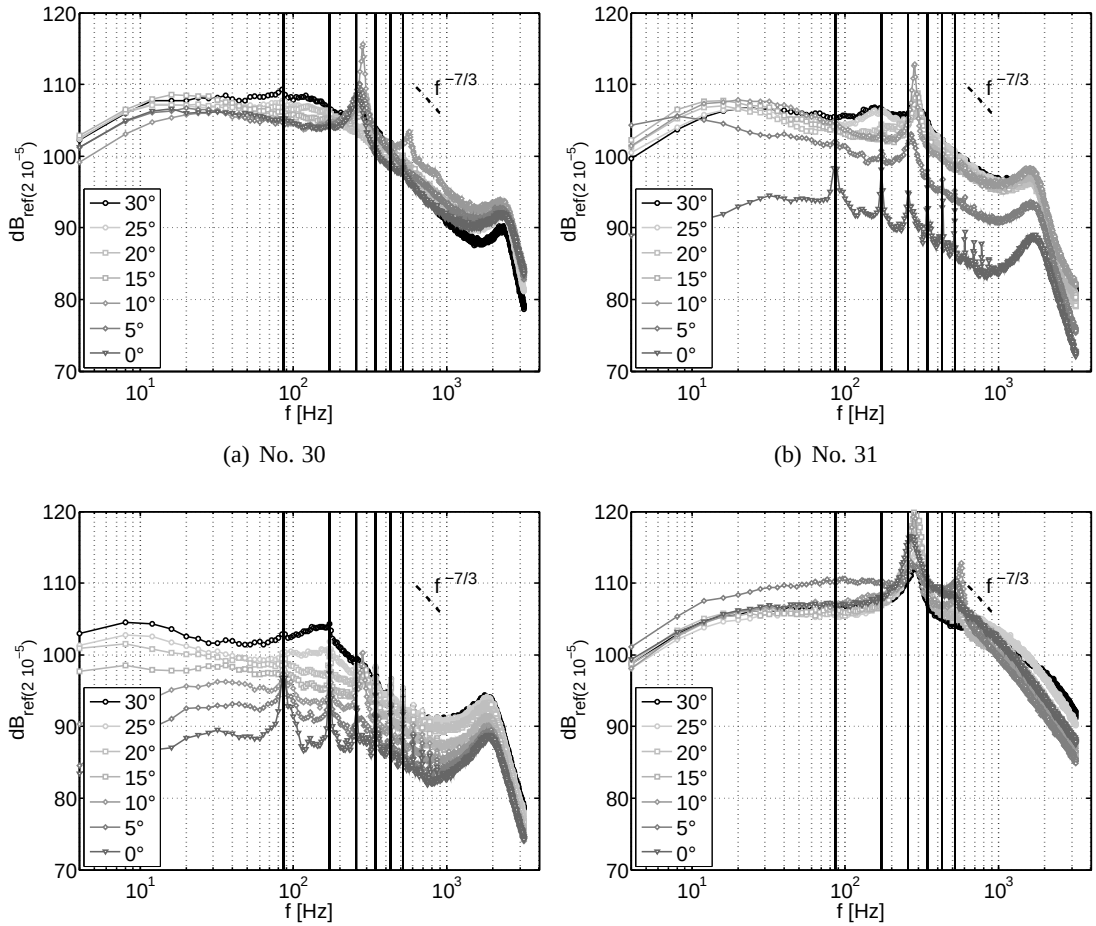

(a) No. 30 (b) No. 31

(c) No. 32 (d) No. 37

Figure 11. Spectral analysis of different pressure transducers as a function of β

160Hz at yaw angles of $25°$ and $30°$, mainly visible on the autospectra of the transducer No. 31, which still has to be analysed in more detail.

The amplitude change observed on the pressure transducer No. 37 is most likely due to its position in respect to the front lee cylinder wake. As the yaw angle grows the wake is more and more turned away from the measurement point, so that it is less sensible to the vortex shedding.

The variation in amplitude of tap No. 31 on the other hand is believed to be linked to the observations made for the mean flow. At $0°$ yaw the cylinder wake stays under the model and hence has little or no influence on the lateral side. As the angle rises, the cylinder wake interacts with the lateral flow and the peak appears. With a further rise, a lateral vortex (b) is generated due to an interaction of the underbody flow with the free flow and is piloted by the cylinder wake. As the angle becomes larger than approximately $15°$, this longitudinal structure detaches from the body and hence the coherent part of the fluctuations is orientated further away from the body, so that they have less effect on the body forces. This results in a decrease in the induced pressure fluctuations and hence the organised force fluctuation.

This shows that it is mainly the front lee strut that pilots the flow on the lee side and induces coherence into the flow and hence onto the body forces.

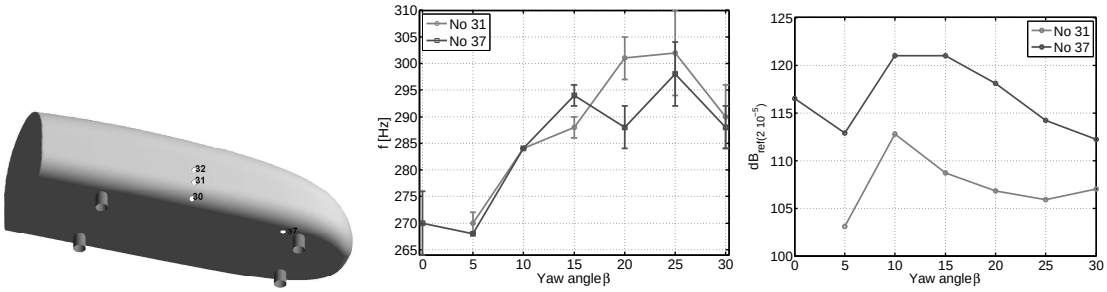

(a) Position of transducers No 30-32 and 37

(b) Peak frequency vs yaw anlge

(c) Peak amplitude vs yaw anlgel

Figure 12. Frequency peak and amplitude analysis as a function of the yaw angle (error bar indicate width of peak maximum)

4. Conclusion

Summarising, the mean flow is characterised by two lee ward vortical structures (a) and (b), shown in Figure 3. The upper vortex (a) plays an important role on the mean forces and is at the origin of a counter rotating yawing moment, created on the upper rear lee side. This moment has a positive effect on the global yawing moment, which it reduces.

The work on the analysis of the force dynamics, as developed in this paper, has shown that a coherent frequency is induced to the model dynamic forces. It is shown that this is linked to the vortex shedding of the cylindrical struts, especially to the wake of the front lee strut. Furthermore, the frequency and the amplitude of this shedding phenomenon, are shown to depend on the yawing angle. The amplitude reaches its maximum around 15° at a frequency around 290Hz for the pressure measurements and 317Hz for the numerical simulation.

The wind tunnel measurements indicate that the frequency rises with the yaw angle. Beyond 20° the frequency stays fairly constant around 295Hz, but the amplitude decreases further. This phenomena is explained by the analysis from the steady flow, more precisely it is linked to the flow structure (b). This longitudinal vortex detaches from the model at yaw angles larger than 15°, hence causing less coherence in the dynamic forces.

So in the dynamic analysis it is not the upper vortex, that plays a predominant role at high yaw angles, as it is the case for the mean force, but it is especially the lower vortex that is strongly interacting with the front lee strut and has the most effect in the mid yaw angle range.

References

1 Chometon, F. et al.: Experimental Analysis of Unsteady Wakes on a New Simplified Car Model. *Bluff Body Aerodynamics and Applications Congress*, Ottawa (2004)

2 Gohlke, M. et al. Experimental analysis of flow structures and forces on a 3D-bluff-body in constant cross-wind, *Exp. Fluids* (2007) (submitted)

3 Gilhaus, A.M. & Renn,V.E.: Drag and Driving-Stability-Related Aerodynamic Forces and Their Interdependence - Results of Measurements on 3/8-Scale Basic Car Shapes. In: *SAE, Society of Automotive Engineers*, Warrendale, Pa. (1986)

4 Howell, J.P.: Shape Features which Influence Crosswind sensitivity. In: *Vehicle Ride and Handling conf., I. Mech. E. Paper C466/036/93 1993*

5 Monin, A.S & Yaglom A.M.: Statistical Fluid Mechanics. *vol. II, MIT Press* (1975)